Journal of Physics: Conference Series

The effect of Vanadium dopant on Bandgap Energy of $Ni_{1-x}V_xFe_2O_4$ nanospinel

The effect of Vanadium dopant on Bandgap Energy of $Ni_{1-x}V_xFe_2O_4$ nanospinel

R Situmeang[1*], A A Saputra[1], Y Andayani[1], M I Imanudin[1], and S Sembiring[3]

[1] Department of Chemistry, Faculty of Mathematics and Natural Sciences, University of Lampung, Jl. Sumantri Brodjonegoro no 1, Bandar Lampung 35145, Indonesia
[2] Department of Physics, Faculty of Mathematics and Natural Sciences, University of Lampung, Jl. Sumantri Brodjonegoro no 1, Bandar Lampung 35145, Indonesia

Corresponding email: rudy.tahan@fmipa.unila.ac.id

Abstract: V^{n+} doped $NiFe_2O_4$, $Ni_{1-x}V_xFe_2O_4$ (where x = 0.1, 0.3, and 0.5) nanomaterials were synthesized by sol-gel and freeze drying method simultaneously using nitrates of iron, and nickel, and ammonium vanadate as the starting materials. Powder X-ray Difraction (XRD) showed that all composition was found to have cubic spinel, hexagonal and monoclinic structure. The average crystallite size using scherrer calculation was found to be in the range of 20 - 42 nm. The band gap energy (Eg) of undoped $NiFe_2O_4$ was estimated to be 1.9 eV from UV-Vis diffuse reflectance spectroscopy (DRS). With the increase of V^{n+} dopant, the Eg value both decreased and increased from 1.6 eV to 2.0 eV, due to the difference of particle size of the samples.

Keywords: spinel, nanomaterial, dopant, bandgap energy

1. Introduction

Until now, the modification of the AB_2O_4 nano spinel structure with the tetrahedral site A as the +2 valence cation and the octahedral site B as the +3 valence cation is still very interesting and has been widely carried out by researchers considering the unique properties possessed by these nano spinel compounds through substitution of cations A or B into $A'B_2O_4$ or AB'_2O_4 or partial substitution to $A_{1-x}A'_xB_2O_4$ or A $(B_{1-y}B'_y)_2O_4$ or $A_{1-z}A'_zBB'O_4$ [1-5]. This modification can give the normal spinel or inverted spinel structure where the +3 cation fills the tetrahedral site and the oxygen occupies a face-centered cube position in a tightly packed arrangement [6, 7]. One of these spinel materials is $NiFe_2O_4$ nanomaterial which has many benefits in the field of catalysis [8, 9], magneto-optics [10, 11], supercapacitors [12, 13], photocatalytic [14, 15], and electronic devices [16, 17].

In the field of catalysts, the utilization of nanospinel nickel ferrite, $NiFe_2O_4$, is studied based on the unique properties of Lewis and Bronsted-Lowry [18, 19] acidity, surface area [20, 21], thermal and chemical stability [22, 23], oxygen mobility [24, 25] and adsorption-desorption [26, 27]. As for photocatalytic applications, in addition to the characteristics discussed earlier, a very needed property is the ease of promoting electrons from the valence band (HOMO) to the conductance band (LUMO). The easier to promote the electrons the less energy required or in other words, the distance between the valence band and the conductivity band is closer [28, 29].

The electrons promotion from the upper valence band to the lowest conduction band requires a minimum energy equivalent to the band gap energy (Eg). If the band gap energy is zero (E_g = O eV) or large (E_g > 4 eV), then they are either a metal or an insulator, respectively. If the band gap energy is between 0 and 4.0 eV, then the metal oxides or composites is a semiconductor. Furthermore, band gap energy is classified as direct and indirect. Direct means that the minimum energy of the lowest

conduction band is just above the maximum energy of the valence band at the same crystal momentum. If this is not, it is called the indirect band gap energy, as shown in Figure 1 below.

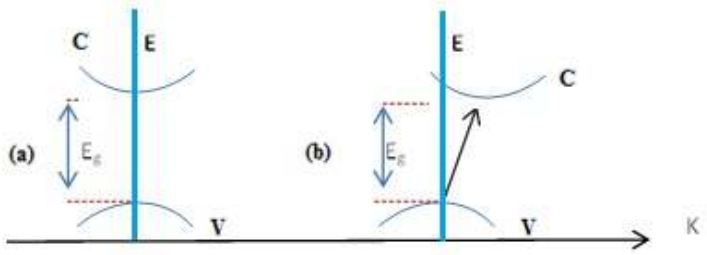

Figure 1. Schemes of band gap energy : (a) direct and (b) indirect transitions which are allowed

The UV-Visible diffuse - reflectance spectrophotometer is a viable tool for the use of a simple method based on the Kubelka-Munk theory [30] and the Tauc [31] plot to obtain the band gap energy. Mathematically, the equation is expressed as follows: $\alpha h\nu = \beta\ (h\nu - Eg)^n$, where h is the Planck constant (J. s^{-1}), β the absorption constant, ν is the frequency of light (s^{-1}), E_g is band gap energy (eV), and n with respect to the types of electron transitions that are possible. The value of n is 2 for the allowed indirect transition, 3 for the forbidden indirect transition, ½ for the directly allowed transition, and 3/2 for the forbidden direct transition.

The impact of adding dopants to a nanospinel can decrease or increase the energy band gap even though it is still in the $0 < Eg < 4.0$ eV range. If the addition of dopants to a nanospinel material decreases the band gap energy, a redshift will occur. But if the addition of dopant increases its bandgap energy, there will be a blue shift where the band gap energy magnitude will be related to the range of wave numbers used in the application [32, 33]

On this chance, we reported the effect of Vanadium dopant on band gap energy of $Ni_{1-x}V_xFe_2O_4$ using the sol gel method and its possible application in photocatalytic reaction by analyzing the material using Diffuse Reflectance UV-Vis Spectroscopy, and X-Ray Diffraction for knowing its crystalline phases formed and crystallite size.

2. Experimental

2.1. Material

The materials used in this study were $Ni(NO_3)_2 . 6\ H_2O$ (Merck, 99%), $Fe(NO_3)_3 . 9\ H_2O$ (Merck, 99%), NH_4VO_3 (Merck, 99%), pectin and distilled water.

2.2. Instruments

The instruments used for characterization include X-Ray Diffraction (XRD) model PW 1710 with Cu-Kα radiation for structure identification, and Diffuse Reflectance UV-Vis Spectroscopy (Agilent Cary 60) to determine the band-gap energy.

2.3. Preparation of $Ni_{1-x}V_xFe_2O_4$

The nanocatalyst was prepared by dissolving 8 grams of pectin in distilled water 400 mL using a magnetic stirrer at room temperature to obtain a homogeneous solution for around 4 hours. 25-30 mL Ammonia is added to reach pH of 11. For example, to prepare $Ni_{0.8}V_{0.2}Fe_2O_4$ as an example, then put the Ni-nitrates solution (1.994 g in 150 mL distilled water), Fe-nitrates solution (6.9407 g in 350 mL distilled water), and ammonium vanadate solution (0.2009 g in 100 mL destilled water)and poured

slowly and simultaneously using an infusion tube, while continuing to stir until homogeneous. Then heated while continuing to stir using a heating magnetic stirrer at a temperature of 80 °C, until the precursor of $Ni_{(1-x)}VxFe_2O_4$ gel was obtained. The gel was dried with a freeze dryer for 24-48 hours and then calcined at 600 °C for 10 hours. The nanomaterial $Ni_{(1-x)}$ $V_xFe_2O_4$ was obtained and ready to analyze.

2.4. Characterization of $Ni_{1-x}V_xFe_2O_4$

2.4.1. X-Ray Diffraction Analysis

The X-ray diffraction pattern $Ni_{1-x}V_xFe_2O_4$ was recorded at 2θ = 10-90º using a Philips diffractometer model PW 1710 Cu-Kα radiation. Phase identification was carried out by matching the diffractogram of the sample to the standard diffractogram using the JCPDF published by ICCD PDF. The crystallite size was determined by the Scherrer method [34].

2.4.2. UV-Vis DR Spectroscopy Analysis

Determination of the $Ni_{1-x}V_xFe_2O_4$ band-gap energy, a number of samples were analyzed using UV-Vis Diffuse Reflectance Spectroscopy and scanned at a wavelength of 200-800 nm [30].

3. Results and Discussion

3.1. Structural Analysis of X-Ray Diffractogram

Based on the results of the diffractogram analysis that has been carried out by the Rietveld calculation, as shown in Figure 2 below, it can be said that $Ni_{0.9}V_{0.1}Fe_2O_4$ spinels are formed and the vanadium cation is in the $NiFe_2O_4$ spinel structure. Furthermore, the increase in the number of vanadium cations added to $Ni_{1-x}V_xFe_2O_4$ has an impact on the formation of the V_2O_5 and Fe_2O_3 crystalline phases as described in the previous article [35].

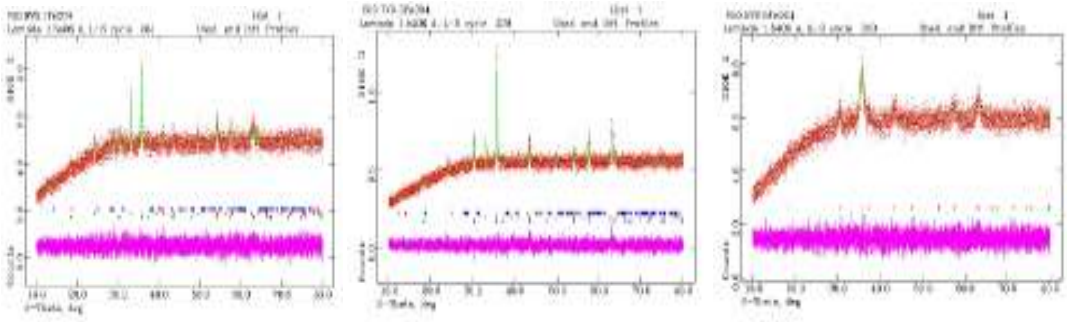

Figure 2. Difractogram of $Ni_{1-x}V_xFe_2O_4$ nanospinel {where (a) x=0.1, (b) x=0.3, and (c) x=0.5}

Furthermore, by using the Scherrer method to calculate the crystal size [34], it was found that the crystal size of $Ni_{0.9}V_{0.1}Fe_2O_4$, $Ni_{0.7}V_{0.3}Fe_2O_4$, and $Ni_{0.5}V_{0.5}Fe_2O_4$, respectively 20.87, 42.08, and 39.97 nm as shown in the previous article [35].

3.2. Analysis of UV-Visible DRS Spectrum

To give the significant information in relation to the effect of crystallite size on the band gap energy (E_g) of spinel $Ni_{1-x}V_xFe_2O_4$ samples, UV-Visible diffuse reflectance spectroscopy (DRS) analysis was carried out. The *E*g of the samples can be evaluated using the Kubelka-Munk method [30].

Optical absorption bands were detected on $Ni_{1-x}V_xFe_2O_4$ nanospinel through the absorbance spectra of UV-Visible DRS versus the wavelength as shown in Figure 3 below, where the five bump or peaks at wavelengths of about 360, 460, 560, 630 and 750 nm show absorption peaks. The peaks indicate that there is an interaction between the 3d Fe^{3+} , 3d Ni^{2+} and the 3d V^{3+} orbitals with the 2p O^{2-} orbitals, respectively, which are shown at the 360, 460 and 560 nm wavelengths of absorption, respectively. Most probably week absorption bands at 630 and 750 nm belongs to d-d transition in Fe^{3+} and Ni^{2+}/V^{3+} ions in an octahedral and tetrahedral symmetries [22], *which are influenced by replacing Ni with V in* $Ni_{1-x}V_xFe_2O_4$ *nanospinel.* Intra-atomic d-d transitions are of much lower intensity comparison to the inter-atomic transitions at region of fundamental absorption edge, as the amount of vanadium dopant more increase.

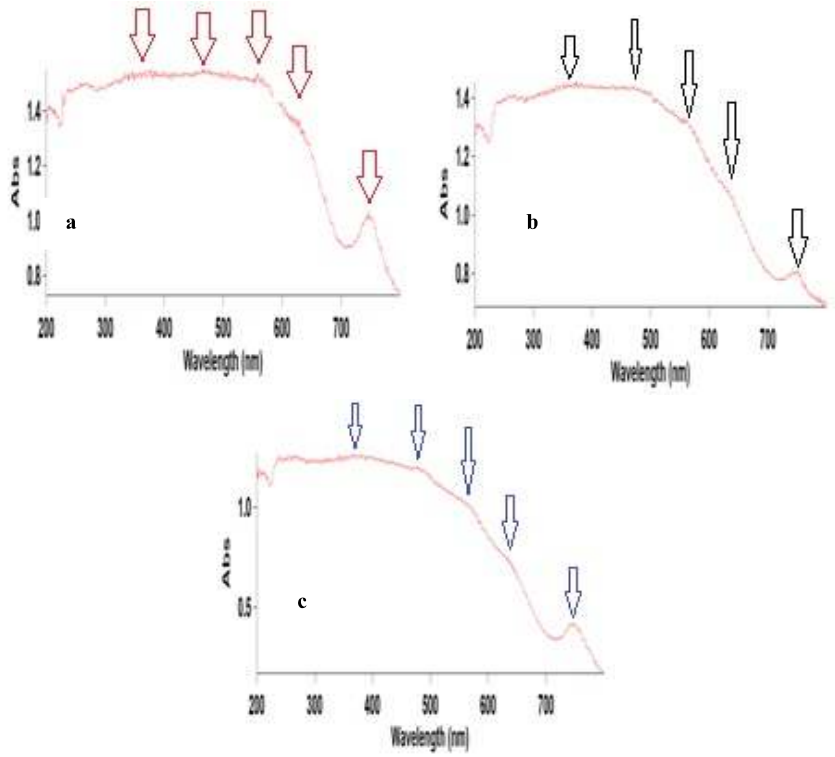

Figure 3. UV-Vis DR Absorption Spectra of $Ni_{1-x}V_xFe_2O_4$ where (a) x = 0.1; (b) x=0.3; and (c) x=0.5

The calculated E_g for all compositions of spinel $Ni_{1-x}V_xFe_2O_4$ (where x = 0.0, 0.1, 0.3, and 0.5) nanomaterials are 1.9, 1.6, 1.8, and 2.0 eV, respectively [35]. It is inferred that there is a decrease and an increase in the E_g of doped samples, when compared to the undoped $NiFe_2O_4$. The E_g value of undoped $NiFe_2O_4$ is 1. 9 eV, and hence, there is a red shift for x = 0.1, and 0.3 and blue shift for x = 0.5 of V_x-doped $Ni_{1-x}Fe_2O_4$ samples. Chavan and Naik [36] found a different value (2.82 eV) for undoped $NiFe_2O_4$ sample and increased as the amount of Mg dopant increased. The decrease in band gap energy may also be due to the sp-d exchange interaction between the localized d-electrons of V^{3+}/Ni^{2+} ions and band electrons of spinel $NiFe_2O_4$ [22].

4. Conclusion

Based on the analysis of $Ni_{1-x}V_xFe_2O_4$ nanomaterial characteristics, it can be concluded that the addition of vanadium dopant into $NiFe_2O_4$ nanospinel affected on the structure of $NiFe_2O_4$ nanospinel where if the amount of vanadium dopants increases the crystalline phase of $NiFe_2O_4$ decreases due to the formation of other crystalline phases such as hexagonal Fe_2O_3 and monoclinic V_2O_5. Furthermore, the greater the amount of vanadium dopant added, the greater the crystalline size formed but the band gap energy more shifted to red and less shifted to blue.

Acknowledgements

We really thank to the Research Directorate and Social Services , Research Deputy and the Ministry of Research Development and Technology/National Research Institution and Innovation (BRIN) and the Research Institution of University of Lampung (LPPM) for research funding provided through the Competitive Research Grant, with research contract Num. 179/SP2H/AMD/LT/DRPM/2020 and the Integrated Services Unit of Integrated Laboratory and the Technology Innovation Centre, the University of Lampung for analyzing the samples.

References

[1] Hema E, Manikandan A, Karthika P, Arul Antony S, Venkatraman B R. 2015. A Novel Synthesis of Zn^{2+}-Doped $CoFe_2O_4$ Spinel Nanoparticles: Structural, Morphological, Opto-magnetic and Catalytic Properties. *J. Supercond. Nov. Magn*., DOI 10.1007/s10948-015-3054-1

[2] Yuvaraj S, Selvan R K, and Lee Y S. 2016. An overview of AB_2O_4- and A_2BO_4-structured negative electrodes for advanced Li-ion batteries. *RSC Adv.*, 6 (26), 21448-21474

[3] dos Santosa, M E, Ferreira R A, Lisboa-Filhoc P N, Pen˜a O. 2013. Cation distribution and magnetic characterization of the multiferroic cobaltmanganese Co_2MnO_4 spinel doped with bismuth. *J. Magn. Magn. Mater*., 329, 53–58

[4] Muruganantham R, Lu J-S, Maggay I V B, Chang B K, Wang P K, Liu W-R. 2020 Modification of spinel-based CoV_2O_4 materials through Mn substitution as a potential anode material for Li-ion storage. *Surf. Coat. Techn*., 389, 125602. https://doi.org/10.1016/j.surfcoat.2020.125602

[5] Maiti S, Sclar H, Rosy, Grinblat J, Talianker M, Burstein L, Noked M, Markovsky B, and Aurbach D. 2020. Modification of Li- and Mn-Rich Cathode Materials *via* Formation of the Rock-Salt and Spinel Surface Layers for Steady and High-Rate . Electrochemical Performances. *ACS Appl. Mater. Interfaces*, 12(29), 32698–32711

[6] Bhattacharya J, and Wolverton C. 2013. Relative stability of normal *vs.* inverse spinel for 3d transition metal oxides as lithium intercalation cathodes . *Phys. Chem. Chem. Phys.*, 15 (17), 6486-6498

[7] Sarkar B, Dalal B, Ashok V D, Chakrabarti K, Mitra A, and De S K. 2014. Magnetic properties of mixed spinel $BaTiO_3$-$NiFe_2O_4$ composites. *J. Appl. Phys.* 115, 123908 ; https://doi.org/10.1063/1.4869782

[8] Mapossa A B, Dantas J, Silva M R, Kiminami R H G A, Costa A C F M, Daramola M O. 2020. Catalytic performance of $NiFe_2O_4$ and $Ni_{0.3}Zn_{0.7}Fe_2O_4$ magnetic nanoparticles during biodiesel production. *Arab. J. Chem.*13(2), 4462-4476. *https://doi.org/10.1016/j.arabjc.2019.09.003*

[9] Hajizadeh Z, Radinekiyan F, Eivazzadeh-Keihan R, and Maleki A. 2020. Development of novel and green $NiFe_2O_4$/geopolymer nanocatalyst based on bentonite for synthesis of imidazole heterocycles by ultrasonic irradiations. *Sci. Rep*.,10, 11671 *https://doi.org/10.1038/s41598-020-68426-z*

[10] Karmakar S, and Behera D. 2020. Magnetic and Optical Studies of $NiFe_2O_4$ Micro- and Nanoparticles. *J. Supercond. Nov. Magn.* , 33, 1619–1627.

[11] Tan J, Zhang W, Xia A-L. 2013. Facile synthesis of inverse spinel $NiFe_2O_4$ nanocrystals and their superparamagnetic properties. *Mat. Res*.,16 (1), 237-241. *http://dx.doi.org/10.1590/S1516-14392012005000157*

[12] Wang Q, Gao H, Qin X, Dai J, and Li W. 2020. Fabrication of $NiFe_2O_4$@$CoFe_2O_4$ core-shell nanofibers for high-performance supercapacitors. *Mater. Res. Express* 7, 015020. *https://doi.org/10.1088/2053-1591/ab61ba*

[13] Ghasemi A, Kheirmand M, and Heli H. 2019. Synthesis of Novel $NiFe_2O_4$ Nanospheres for High Performance Pseudocapacitor Applications. *Rus. J. Electrochem.* 55, 206–214

[14] Ojemaye M O, Okoh O O, and Okoh A I. 2017. Performance of $NiFe_2O_4$-SiO_2-TiO_2 Magnetic Photocatalyst for the Effective Photocatalytic Reduction of Cr(VI) in Aqueous Solutions. *J. Nano Mater.* 2017, 5264910 . *https://doi.org/10.1155/2017/5264910*

[15] Tsvetkov M P, Ivanova I R, Valcheva E P, Zaharieva J Ts, Milanova M M. 2019. Photocatalytic activity of $NiFe_2O_4$ and $Zn_{0.5}Ni_{0.5}Fe_2O_4$ modified by Eu(III) and Tb(III) for decomposition of Malachite Green *De Gruyter Open Chem.,* 2019; 17: 1124–1132. *https://doi.org/10.1515/chem-2019-0116*

[16] Lüders U, Barthelemy A, Bibes M, Bouzehouane K. 2006. $NiFe_2O_4$: A Versatile Spinel Material Brings New Opportunities for Spintronics. *Adv.Mater.* 18(13),1733 – 1736. DOI: 10.1002/adma.200500972

[17] Yadav R S, Kuřitka I, Vilcakova J, Skoda D, Urbánek P, Machovsky M, Masař M, Kalina L, Havlica J. 2019. Lightweight $NiFe_2O_4$-Reduced Graphene Oxide-Elastomer Nanocomposite flexible sheet for electromagnetic interference shielding application. *Comp. Part B: Eng.*, 166, 95-111. *https://doi.org/10.1016/j.compositesb.2018.11.069*

[18] Tiwari R, De M,Tewari H S, Ghoshal S K. 2020. Structural and magnetic properties of tailored $NiFe_2O_4$ nanostructures synthesized using auto-combustion method. Res. Phys. 16, 102916. *https://doi.org/10.1016/j.rinp.2019.102916*

[19] Benrabaa R, Boukhlouf H, Barama S, Bordes-Richard E. 2012. Structural, Textural and Acid–Base Properties of Nano-Sized $NiFe_2O_4$ Spinel Catalysts. *Catal. Lett.* 142 (1), 42-49. DOI: 10.1007/s10562-011-0726-8

[20] Özçelik B, Özçelik S, Amaveda H, Santos H, Borrell C J, Sáez-Puche R, de la Fuente G F, Angurel L A. 2020. High speed processing of $NiFe_2O_4$ spinel using a laser furnace. *J. Mater.* 6(4), 661-670. *https://doi.org/10.1016/j.jmat.2020.05.003*

[21] Kumar P V, Short M P, Yip S, Yildiz B, and Grossman J C. 2013. High Surface Reactivity and Water Adsorption on $NiFe_2O_4$ (111) Surfaces. *J. Phys. Chem. C*, 117(11), 5678–5683. *https://doi.org/10.1021/jp309434a*

[22] Tong S-K, Chi P-W, Kung S-H, Wei D H. 2018. Tuning bandgap and surface wettability of $NiFe_2O_4$ driven by phase transition. *Sci. Rep.* 8, 1338.

[23] Salazar-Tamayo H, Tellez K E G, Meneses C A B. 2019. Cation Vacancies in $NiFe_2O_4$ During Heat Treatments at High Temperatures: Structural, Morphological and Magnetic Characterization. *Mat. Res*., 22 (5), 0298. *https://doi.org/10.1590/1980-5373-mr-2019-0298*

[24] Lim D, Kong H, Kim N, Lim C, Ahn W-S, Baeck, S-H. 2019. Oxygen-Deficient $NiFe_2O_4$ Spinel Nanoparticles as an Enhanced Electrocatalyst for the Oxygen Evolution Reaction. *ACES Chem. nano mat*., 5 (10), 1296-1302. *https://doi.org/10.1002/cnma.201900231*

[25] Nagarajan V, and Chandiramouli R. 2006. 2017. Investigation on nickel ferrite nanowire

device exhibiting negative differential resistance—a first-principles investigation. *Cond. Mat. Phys.*, 20(2), 23301:1-12. DOI:10.5488/CMP.20.23301

[26] Kumar P V, Short M P, Yip S, Yildiz B. 2013. High Surface Reactivity and Water Adsorption on $NiFe_2O_4$ (111) Surfaces. *J. Phys. Chem. C* 117(11), 5678–5683. DOI: 10.1021/jp309434a

[27] Rigoa C, da Cruz Severoa E, Mazuttia M A, Dottoa G L, Jahna S L, Gündelb A, Luccheseb M M, Chiavone-Filhoc O, Foletto E L. 2017. Preparation of Nickel Ferrite/Carbon Nanotubes Composite by Microwave Irradiation Technique for Use as Catalyst in Photo-Fenton Reaction. *Mater. Res.* 20(Suppl. 2), 311-316. DOI: http://dx.doi.org/10.1590/1980-5373-MR-2016-0672

[28] Yan H, Wang X, Yao M, and Yao X. 2013. Bandstructure design of semiconductors for enhanced photocatalytic activity : The case of TiO_2. *Prog. Nat.Scie. : Mater. Inter.*, 23(4), 402 – 407

[29] Khairy M, and Zakaria W. 2014. Effect of metal-doping of TiO_2 nanoparticles on their photocatalytic activities toward removal of organic dyes. *Egyp. J.Petrol.*, 23, 419 – 426

[30] Sangiorgi N, Aversa L, Tatti R, Verucchi R, and Sanson A. 2017. Spectrophotometric method for optical band gap and electronic transitions determination of semiconductor materials. *Opt.Mater.*, 64, 18 – 25.

[31] Liu P, Longo P, Zaslavsky A, and Pacifici D. 2018. Optical bandgap of single and multiple layered amorphous gemanium ultra thin films. *J. Appl. Phys.*, 119, 014304-1 – 014304-9.

[32] Chen J, Wang Y, and Deng Y. 2013. *J. Alloys Compd.* 552, 65

[33] Krishnan D, Boddapati L, Pachauri N, Gupta A. 2014. Probing optical band gaps at the nanoscale in $NiFe_2O_4$ and $CoFe_2O_4$ epitaxial films by high resolution electron energy loss spectroscopy. *J. Appl. Phys.* 116(10):103505-103505-8. DOI: 10.1063/1.4895059

[34] Cullity, B. D. 1978. *Elements of X-ray Diffraction,* 2nd ed., Addison-Wesley, London, p.102.

[35] Situmeang R, Romiyati R, Simanjuntak W, Yuwono S D, Sembiring S. 2020. $Ni_{1-x}V_xFe_2O_4$ Nano photocatalysts: The effect of Vanadium addition into its activity on Remazol Golden Yellow Degradation under visible light Irradiation. submitted and processed in *J.Nano Mater.*

[36] Chavan P, and Naik L R. 2017. Investigation of energy band gap and conduction mechanism of magnesium substituted nickel ferrite nanoparticles. *Phys. Stat. Sol.A*, 1700077. DOI 10.1002/pssa.201700077